

Ab initio simulation of band-to-band tunneling FETs with single- and few-layer 2-D materials as channels

Áron Szabó*, Cedric Klinkert*, Davide Campi†, Christian Stieger*, Nicola Marzari†, and Mathieu Luisier*

*Integrated Systems Laboratory, ETH Zürich, 8092 Zürich, Switzerland

†Laboratory of Theory and Simulation of Materials, EPFL, 1015 Lausanne, Switzerland

(Invited Paper)

Abstract—Full-band atomistic quantum transport simulations based on first principles are employed to assess the potential of band-to-band tunneling field-effect-transistors (TFETs) with a 2-D channel material as future electronic circuit components. We demonstrate that single-layer transition metal dichalcogenides (TMDs) are not well-suited for TFET applications. There might, however, exist a great variety of 2-D semiconductors that have not even been exfoliated yet: this work pinpoints some of the most promising candidates among them to realize highly efficient TFETs. Single-layer SnTe, As, TiNBr, and Bi are all found to ideally deliver ON-currents larger than $100 \mu\text{A}/\mu\text{m}$ at 0.5 V supply voltage and 0.1 nA/ μm OFF-current value. We show that going from single to multiple layers can boost the TFET performance as long as the gain from a narrowing band gap exceeds the loss from the deteriorating gate control. Finally, a 2-D van der Waals heterojunction TFET is revealed to perform almost as well as the best single-layer homojunction, paving the way for research in optimal 2-D material combinations.

Index Terms—Device simulation, TFET, 2-D materials, *ab initio*, quantum transport

I. INTRODUCTION

ONE of the main challenges in electronics nowadays consists in reducing the energy consumption of the myriads of microprocessors that build the core of consumer products and the Internet of Things (IoT). In order to make future developments sustainable, the supply voltage V_{DD} of metal-oxide-semiconductor field-effect transistors (MOSFETs) - the active components of all digital logic circuits - should be significantly reduced, while providing the same current magnitude to maintain high speed operations. The performance of conventional MOSFETs is however bounded by the 60 mV/dec theoretical limit of their inverse subthreshold slope (SS) at room temperature. As a consequence, a gate voltage change ΔV_g of at least 60 mV must be applied to increase the drive current I_d by one order of magnitude. The ratio between the ON-state current I_{ON} and the leakage current in the OFF-state, I_{OFF} , is therefore limited. Since the semiconductor industry is rapidly approaching the maximum I_{ON}/I_{OFF} ratio possible in MOSFETs, novel device types relying on operating mechanisms different from thermionic emission are under intense investigation [1].

Band-to-band tunneling field-effect transistors (TFETs) are promising candidates for that purpose, as their working principle is based on the injection of cold instead of hot carriers, effectively creating a band-pass filter for the high energy

electrons that limit the performance of MOSFETs [2]. The abrupt opening and closing of a tunneling window with high transmission probability requires an excellent electrostatic control that is favored by multi-gate, three-dimensional device structures over planar ones with a single gate contact. Hence, Silicon and III-V gate-all-around nanowire TFETs have been demonstrated to break the 60 mV/dec thermal limit of MOSFETs, but with very low ON-currents [3], [4], [5]. Tunneling transistors with I_{ON} 's suitable for practical applications have been fabricated as well [6], [7], [8], but without simultaneously exhibiting a steep SS. At this point, delivering a high ON-current and bringing SS well below 60 mV/dec remains an arduous objective. To the best of our knowledge, a recently reported InAs/InGaAsSb/GaSb nanowire TFET with $I_{ON} = 10.3 \mu\text{A}/\mu\text{m}$ and $I_{OFF} = 1 \text{ nA}/\mu\text{m}$ at $V_{DD} = 0.5 \text{ V}$ [9] represents one of the most impressive and promising achievements to date. In spite of that, this solution remains far from reaching the level of performance of Si MOSFETs.

Following the first demonstration of a monolayer MoS₂ transistor [10], the research in single- and few-layer two-dimensional (2-D) semiconductors has undergone a veritable boom. As part of this on-going effort, TFETs with a 2-D channel material have started to emerge as an alternative to traditional semiconductors. The motivation beyond such investigations can be traced back to the unique features of 2-D materials that can be leveraged in tunneling devices: (1) the extraordinary gate control offered by channels with ultra-scaled thicknesses (<1 nm), (2) the variety of the members of the 2-D material family, (3) the large design space that combinations of 2-D layers opens up, and (4) the possibility to create heterojunctions with fine-tuned band alignments and defect-free interfaces thanks to naturally passivated surfaces and the absence of dangling bonds [11].

Surfing on this wave, several simulation approaches and design tools have been developed to shed light on the behavior of 2-D TFETs. In this context, single-layer transition metal dichalcogenides (TMDs) [12], [13] and black phosphorus [14] TFETs have been extensively studied through computer models mostly based on the tight-binding (TB) method. Some TMDs, especially WTe₂, were claimed to be able to deliver ON-currents larger than $100 \mu\text{A}/\mu\text{m}$ at $V_{DD} = 0.5 \text{ V}$ and $I_{OFF} = 1 \text{ nA}/\mu\text{m}$. Better device characteristics were predicted by other theoretical studies for TFETs implementing a van der Waals hetero-junction as active tunneling region [15],

[16]. Practical devices have been experimentally realized, confirming the potential of 2-D materials as TFET building blocks [17], [18]. It should however be noticed that the highest ON-current with an inverse subthreshold slope steeper than 60 mV/dec over many orders of magnitudes was achieved by a MoS₂-Ge (2-D to 3-D) heterojunction [17], leaving open the question whether 2-D materials alone are appropriate for TFETs.

To address this issue, we will first revisit the performance of TFETs based on the most popular single-layer TMDs through advanced computational modeling. To go one step further, we will then explore more exotic 2-D materials as possible TFET channels. All of them have been theoretically proved to be stable in vacuum, their electronic properties have been analyzed in great details [19], but they have not been experimentally studied yet. To complete the picture, we will extend our investigation to multi-layer devices and to van der Waals heterojunctions. The focus is set on identifying components with a high ON-current.

A quantum transport simulator relying on the Non-Equilibrium Green's Function (NEGF) formalism and first principles concepts (density functional theory) will be used to give insight into the “current vs. voltage” characteristics of all considered TFETs. This approach avoids the need for empirical parametrizations, hence enabling the inspection of TFETs made of not-yet exfoliated 2-D materials. We will show that none of the widely studied TMD monolayers can reach an I_{ON} larger than approximately $10 \mu A/\mu m$, while some of the recently discovered 2-D materials significantly outperform them. We will also demonstrate that going from single- to few-layer channels can lead to performance enhancement under certain circumstances. Finally, we will present a 2-D heterojunction TFET that exhibits a similar ON-current as the best monolayer homojunction. It is expected that these findings will encourage the search for even better-suited 2-D materials or material combinations for TFET channels; spectacular improvements may occur as we move away from conventional TMDs.

The paper is organized as follows: in Section II, the developed *ab initio* simulation approach is introduced. Simulation results of 2-D TFETs are given in Section III, starting with standard TMDs, then novel 2-D materials, multi-layer channels, and van der Waals heterojunctions to finish. Conclusions are drawn in Section IV.

II. SIMULATION APPROACH

The simulation workflow used in this paper starts with the calculation of the single-particle electronic wavefunctions in the primitive unit cell of the investigated 2-D materials. This is accomplished with the help of density functional theory (DFT) [20] as implemented in the VASP package [21]. The generalized gradient approximation (GGA) of Perdew, Burke, and Ernzerhof (PBE) [22] is utilized in most cases since it has been demonstrated to give a band gap value very close to the experimental one for single-layer MoS₂ [23]. The only exception is black phosphorus (1-, 2-, and 3-layer), where the HSE06 hybrid functional [24] is employed due to its

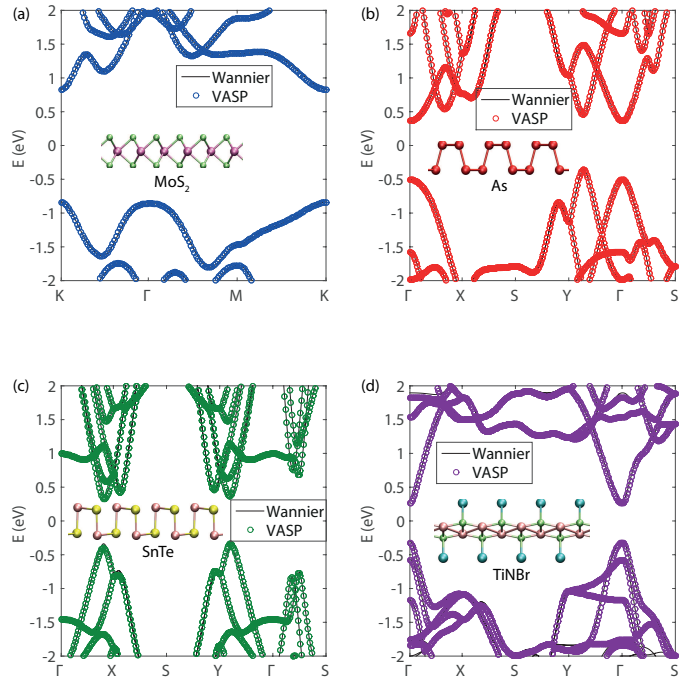


Fig. 1. Bandstructures of selected single-layer materials obtained from VASP (circles) and from sparse MLWF Hamiltonians after applying a cutoff radius of about 15 \AA to the interactions between different Wannier functions (lines): (a) MoS₂, (b) As, (c) SnTe, (d) TiNBr. The MLWF Hamiltonians capture all relevant features for transport calculations with high fidelity. The corresponding crystal structures are shown as insets.

better reproduction of the experimental band gap as compared to PBE that severely underestimates it. It should be pointed out that there is no consensus on the band gap of most 2-D materials. Supposedly more accurate G_0W_0 calculations predict, for example, $E_g=2.78 \text{ eV}$ for MoS₂ [25]. Such large corrections could have a negative influence on the results presented in this paper that can be seen as best case scenarios.

An 500 eV plane-wave cutoff energy, a $25 \times 25 \times 1$ Monkhorst-Pack k -point grid, and 20 \AA out-of-plane vacuum separation are applied to every DFT simulation. Spin-orbit coupling is neglected. The convergence criteria is set to less than 10^{-3} eV/\AA forces acting on each ion and a total energy difference smaller than 10^{-3} eV between two consecutive self-consistent field iterations. In the case of multilayer structures, van der Waals interactions are included through the DFT-D2 method of Grimme [26]. Heterojunctions are modeled in a common unit cell with the average of the lattice parameters of the individual layers. The resulting stress (compressive for one layer, tensile for the other) does not exceed 2%.

The Bloch wavefunctions produced by VASP for a structure without any applied electric field are then transformed into a set of maximally localized Wannier functions (MLWFs) by the Wannier90 tool [27]. The Hamiltonian matrix elements in this basis correspond to interactions between well-localized wavefunctions typically centered on ions. Due to this localization, interactions between Wannier functions separated by a distance larger than a pre-defined cutoff radius can be safely neglected. This cutoff radius is determined on a case-by-case basis to minimize the computational burden, while maintaining

a high accuracy. Its typical value lies in the range of 15 Å. The Hamiltonian matrices of 80 nm long TFETs are built up from the retained matrix elements. They exhibit a block-tri-diagonal structure with a tight-binding-like sparsity pattern. They can be loaded into a ballistic quantum transport solver relying on the Non-Equilibrium Green's Function formalism [28]. This “up-scaling” procedure is further detailed in Ref. [29] and Appendix A of Ref. [30] for homogeneous materials and in Ref. [31] and Appendix B of Ref. [30] for heterojunctions. The accuracy of the method is confirmed in Fig. 1 for four different single-layer 2-D materials, MoS₂, As, SnTe, and TiNBr. Still, should the bandstructure of these crystals be modified by a strong electric field, it is not clear whether the MLWF Hamiltonian would automatically capture these changes.

The NEGF quantum transport simulator solves the Schrödinger- and Poisson equations self-consistently in the presence of electrostatic boundary conditions imposed by the metallic gates. We construct 80 nm long simulation domains with $L_g = 40$ nm top and bottom gate contacts separated from the channel materials by 3 nm thick high- κ HfO₂ layers with $\epsilon_R = 20$ and an equivalent oxide thickness EOT= 0.6 nm. The source and drain extensions measure approximately $L_s = 13$ nm and $L_d = 26$ nm, the rounding coming from the fact that the total TFET length has to be an integer multiple of the primitive unit cell width Δ_{uc} . These regions are doped with a $N_A = 5 \times 10^{13}$ cm⁻² and $N_D = 5 \times 10^{12}$ cm⁻² acceptor and donor concentrations, respectively, that are modeled as uniformly screened background charges in the Poisson equation. Such an ideal configuration could only be imagined in the context of electrostatic doping resulting from additional metal contacts or from the transfer of charges from another 2-D layer stacked with the actual one [32]. As compared to a more realistic atomistic model explicitly accounting for chemical doping or substitutional impurities, the present scheme offers a “best-case” scenario that is suitable to study the performance limit of a given design. Going beyond this approximation is out of the scope of this paper.

Only *n*-type TFETs are simulated here. Their different source and drain lengths and doping concentrations ensure sharp changes in the electrostatics at the source-channel interface, which maximizes the tunneling probability there, and a more smoothly varying potential on the drain side, thus avoiding tunneling leakage currents. The 2-D materials are treated as flakes with one periodic direction, the out-of-plane one, that induces a *k*-dependence of all computed physical quantities. A total of 15 *k*-points between 0 and π have been found sufficient to represent this direction. The dielectric constants of the TMDs are taken from Ref. [33], whereas those of novel 2-D materials have been computed according to Ref. [34]. The source-to-drain voltage of the TFETs, V_{ds} , is set to 0.5 V and the gate voltage V_{gs} is swept from 0 to 0.5 V. The workfunction of the gate metals is adjusted in each case to set the OFF-current at $V_{gs}=0$ V to $I_{OFF}=0.1$ nA/ μ m. Figure 2 depicts the schematics of the studied tunneling devices as well as a summary of the simulation workflow.

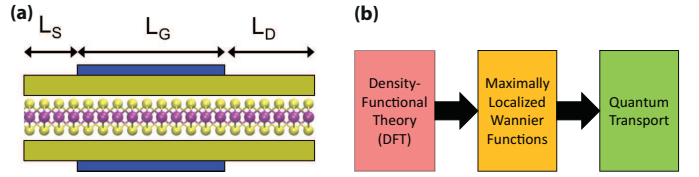


Fig. 2. (a) Schematic view of the considered double-gate TFETs with monolayer 2-D materials as channels. (b) Flow chart of the simulation approach based on density functional theory, maximally localized Wannier functions, and NEGF quantum transport.

III. RESULTS AND DISCUSSION

To illustrate the potential of 2-D materials as active components of future TFETs, the investigated crystals have been divided into four generic categories:

- single-layer transition metal dichalcogenides: MoS₂, MoSe₂, MoTe₂, WS₂, WSe₂, WTe₂ (all of the trigonal prismatic form), and octahedral HfSe₂;
- novel single-layer 2-D materials with small direct band gaps, as predicted by the theoretical study from Ref. [19]: AlLiTe₂, As, Bi, CrSe₂, SnTe, TiNBr, and TiNCl;
- single-, double-, and triple-layer black phosphorus;
- a MoTe₂-SnS₂ van der Waals heterojunction composed of two single-layer crystals.

These four groups will be presented and analyzed one by one in the following subsections.

A. Transition metal dichalcogenides

Molybdenum- and tungsten-based single-layer (SL) transition metal dichalcogenides (TMDs) are all direct gap semiconductors with WSe₂ exhibiting the largest and WTe₂ the smallest theoretical band gap of 1.8 and 0.92 eV, respectively. Note that the trigonal prismatic form of WTe₂, the semiconducting allotrope investigated in this work, is metastable. Reaching high tunneling probabilities requires a small band gap to reduce the tunneling length and small electron/hole effective masses to minimize the decay rate κ along the tunneling path. As Fig. 3 shows, none of the conventional SL 2-D materials fully satisfies these essential criteria. The simulated ON-currents are smaller than 1 μ A/ μ m in all cases, except for WTe₂, where I_{ON} reaches 14 μ A/ μ m. This result is consistent with WTe₂ having the smallest direct band gap and the smallest average electron/hole effective mass in this group, but not sufficient to challenge Si MOSFETs. It should also be emphasized that our drive currents I_d are much smaller than those of Ref. [12]. This could be due to the simulation approach, empirical tight-binding (TB) in Ref. [12] vs. DFT here. There is no guarantee that with a TB method, the imaginary band dispersion responsible for intra- and inter-band tunneling is accurately reproduced, while it is an integral part of DFT bandstructures and their MLWF representation.

Among the considered TMDs, HfSe₂ is the one with the smallest band gap, 0.76 eV, but it is indirect, leading to a reduced transmission probability. Although we only perform ballistic simulations, indirect tunneling can still occur if the transport direction *x* is aligned with the wavevector that connects the minimum of the conduction band (CBmin) and the

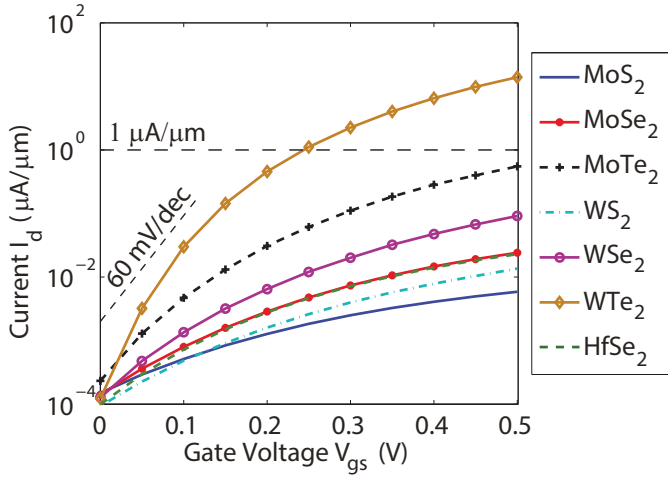


Fig. 3. Transfer characteristics $I_d - V_{gs}$ at $V_{ds} = 0.5$ V of conventional single-layer 2-D materials: MoS₂ (solid line), MoSe₂ (solid line with dots), MoTe₂ (dashed line with crosses), WS₂ (dashed-dotted line), WSe₂ (solid line with circles), WTe₂ (solid line with diamonds), and HfSe₂ (dashed line). The 60 mV/dec slope and the $1 \mu\text{A}/\mu\text{m}$ mark are indicated.

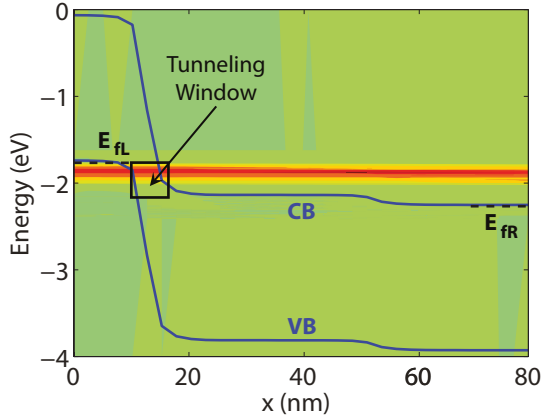


Fig. 4. Spectral current in the OFF-state of the MoS₂ TFET ($V_{gs}=0$ V, $V_{ds}=0.5$ V). Red indicates high current concentrations, green no current. The blue lines refer to the band edges, E_{fL} and E_{fR} to the source and drain Fermi levels, respectively. The black square represents the tunneling window where electrons in the valence band of the source can be ballistically transferred to the conduction band of the channel.

maximum of the valence band (VBmax) of the 2-D material under consideration. This is not the case here since CBmin (VBmax) of HfSe₂ is located at the M (Γ) point and the transport direction x follows the Γ - K axis of the Brillouin Zone. Aligning x with the Γ - M line would require larger unit cells and increased computational burden. For this reason, this case has not been examined here.

Apart from the small ON-currents, it can be observed that almost all TMDs have inverse subthreshold slopes larger than 60 mV/dec despite their excellent electrostatic properties. The only exception is WTe₂, whose SS surpasses the thermal limit. The reason for this behavior is clarified in Fig. 4 that shows the spectral current in the OFF-state of the MoS₂ TFET. To achieve $I_{OFF}=0.1$ nA/ μm , a tunneling window with a significant width must already be available: due to the low tunneling probabilities of MoS₂ and most other TMDs, even the minuscule imposed OFF-current requires a gate voltage

much higher than the one at which the valence band of the source is perfectly aligned with the conduction band of the channel. A sub-thermionic SS can only be expected when this condition is satisfied, that is, in the present case, at negative voltages and not relevant current levels.

The band gaps, electron and hole effective masses, and the computed ON-current values are summarized in Table I situated at the end of the manuscript.

B. Novel single-layer 2-D semiconductors

From the newly generated database of all potentially existing 2-D materials (more than 1,800 compounds) [19], we singled out a few examples with very promising parameters for application as TFET channels. The components with small and direct band gaps have been selected. Still, E_g should not be smaller than 0.5 eV, otherwise turning off the TFET would not be possible at $V_{ds} = 0.5$ V. The material from this group with the largest band gap is AlLiTe₂ with 0.91 eV, which is comparable to WTe₂, while the smallest E_g is obtained for Bi with 0.55 eV. Besides them, the following single-layer crystals are considered: As, CrSe₂, SnTe, TiNBr, and TiNCl.

The transfer characteristics $I_d - V_{gs}$ at $V_{ds} = 0.5$ V of the TFETs made of these materials are shown in Fig. 5. This time, most of the simulated devices reach ON-currents in the range of 100 $\mu\text{A}/\mu\text{m}$ or more, with the exception of the material with the largest gap, AlLiTe₂, and the largest effective masses, CrSe₂. The highest ON-current is found for SnTe, 166 $\mu\text{A}/\mu\text{m}$, one order of magnitude above WTe₂, the best performing TMD. The devices with more than 100 $\mu\text{A}/\mu\text{m}$ ON-currents display clear sub-thermionic operation in the subthreshold regime, with slopes steeper than 60 mV/dec in each case. Bi has the lowest SS thanks to its very low band gap and effective masses. To be able to switch off all these TFETs, the source and drain doping concentrations of the Bi, TiNCl, and TiBrN structures had to be decreased by a factor of 5, 2, and 1.25, respectively. This explains why the current increase in the Bi TFET rapidly saturates compared to the other 2-D materials.

The influence of the effective masses on the device performance is illustrated in Fig. 6, where the complex bandstructure of SnTe and CrSe₂ is displayed. The band gaps of these 2-D materials are almost identical, 0.73 eV for SnTe and 0.75 eV for CrSe₂. The effective masses, however, differ by a factor of 10: both the electron and hole effective masses of SnTe are approximately equal to 0.1 m_0 , while they amount to about 1.0 m_0 in CrSe₂. Hence, the maximum decay rate κ_{max} of the electronic wavefunction inside the band gap of these semiconductors becomes quite different, 1.36 1/nm for SnTe vs. 4.1 1/nm for CrSe₂, roughly a factor $\sqrt{10}$ difference, which corresponds to the square root of the CrSe₂/SnTe effective mass ratio. A high κ_{max} means that the wavefunction of an electron injected into the valence band of the source extension of a TFET rapidly diminishes as it moves towards the conduction band of the channel, thus reducing the tunneling probability, regardless of the band gap value [35]. This is the main reason why CrSe₂ is outperformed by SnTe as well as by every other 2-D material considered in this sub-section.

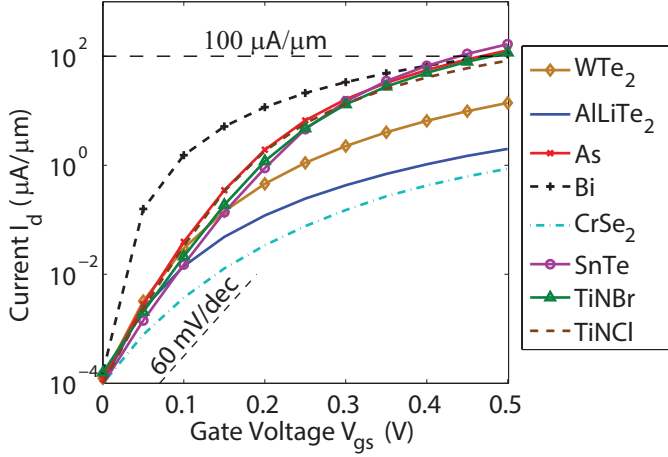


Fig. 5. Transfer characteristics $I_d - V_{gs}$ at $V_{ds} = 0.5$ V of the novel single-layer 2-D materials considered in this work: AlLiTe₂ (solid line), As (solid line with crosses), Bi (dashed line with crosses), CrSe₂ (dashed-dotted line), SnTe (solid line with circles), TiNBr (solid line with triangles), and TiNCl (dashed line). They are compared to WTe₂ (solid line with diamonds).

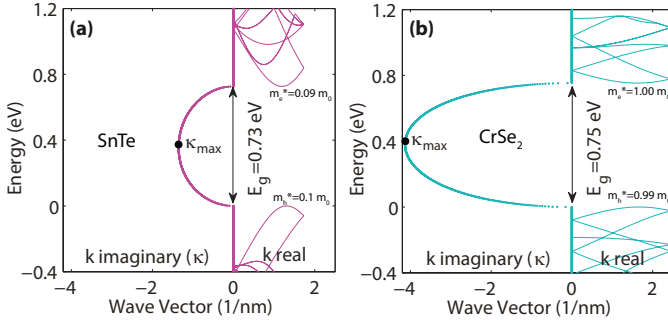


Fig. 6. Complex bandstructure of SL (a) SnTe and (b) CrSe₂. The left axis refers to the imaginary part of the band (energy-resolved decay rate κ) multiplied by a minus sign, the right axis to its real component k . The maximum value of κ , κ_{max} , is indicated for both materials.

C. Single- and few-layer black phosphorus

Exploring novel single-layer 2-D semiconductors is one promising possibility to improve the TFET performance, another one could be the introduction of additional layers to the channel. We will therefore investigate here whether going from single- to few-layer structures offers any benefit. Black phosphorus (BP) is chosen for this task, as its layer-dependent band gap, high mobility, and high anisotropy of the electron and hole effective masses are already well-known [36]. The mass anisotropy can be exploited by orienting the transport axis with the small mass direction, hence combining the advantage of a high electron velocity together with a high density-of-states [37]. A previous theoretical study based on the tight-binding method and an assumed band gap of $E_{g,SL} = 1.4$ eV for the single-layer compound reported ON-state currents larger than $1 \text{ mA}/\mu\text{m}$ at $V_{DD} = 0.5$ V for multi-layer TFETs [14]. Here, $E_{g,SL} = 1.61$ eV and DFT are used.

With this band gap value and relatively large effective masses ($m_e = 0.17$ for electrons and $m_h = 0.16$ for holes), SL BP cannot offer high tunneling currents. Increasing the channel thickness to 2 layers lowers the gap to 1.09 eV, while for 3 layers, it further decreases down to 0.79 eV. The bandstruc-

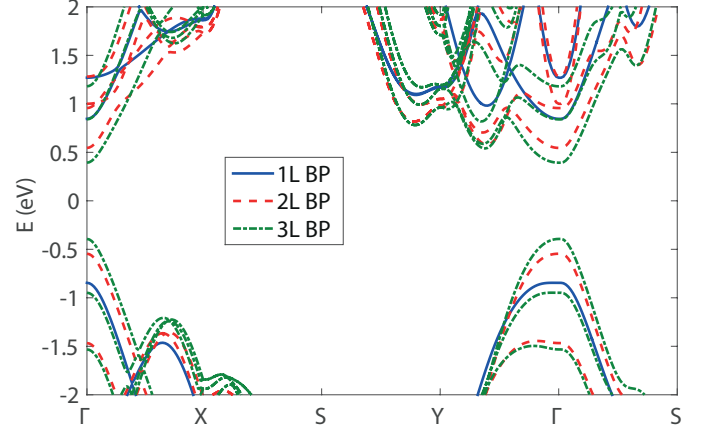


Fig. 7. Bandstructure of single- (solid lines), double- (dashed lines), and tripe-layer (dashed-dotted lines) black phosphorus as computed with DFT and HSE06 functional [24].

tures of BP with 1 to 3 layers are shown in Fig. 7. In each configuration, the band gap remains direct and is located at the Γ point, contrary to most TMDs, where a direct-indirect transition takes place when going from a single- to a multi-layer crystal. Transport occurs along the X direction: only the light electrons and holes of the $\Gamma - X$ path (all in the range between 0.14 and 0.18 m_0) contribute to the tunneling process in the simulated devices.

Thicker channels come at the expense of a reduced electrostatic control. However, as indicated by the transfer characteristics of single-, double-, and triple-layer BP TFETs in Fig. 8, the gain from the smaller gaps overcomes the loss caused by the deterioration of the electrostatics. While the ON-current of SL BP only reaches $0.57 \mu\text{A}/\mu\text{m}$, it increases to $8.3 \mu\text{A}/\mu\text{m}$ in a double-layer and to $58.6 \mu\text{A}/\mu\text{m}$ in a triple-layer BP TFET. This enhancement can be mainly attributed to the narrowing of the band gap. The effective mass variations are smaller than 10 %, whereas the band gap decreases by a factor of two between the single- and triple-layer crystal. These results are better than those obtained for conventional TMDs, but not for SnTe and other novel 2-D semiconductors.

It is not clear whether this ON-current improvement will continue for even thicker channels, and if so, what is the optimal thickness. At one point, by adding more and more layers, the band gap will approach 0.5 eV and the OFF-state leakage will start to exponentially increase. At the same time, the gate control will gradually lose its efficiency, which will affect the subthreshold region. Simulating thicker channels is out of the scope of this work as the computational burden grows very quickly with the cross-section of the device.

D. MoTe₂-SnS₂ van der Waals heterojunction

As last TFET concept, a MoTe₂-SnS₂ van der Waals heterojunction is proposed. The bandstructure of this material combination is depicted in Fig. 9, its device arrangement schematized in Fig. 10 (a). A similar TFET was previously discussed in Ref. [31]. Its structure is slightly different from the one in Fig. 2. The source extension is formed by a p -doped

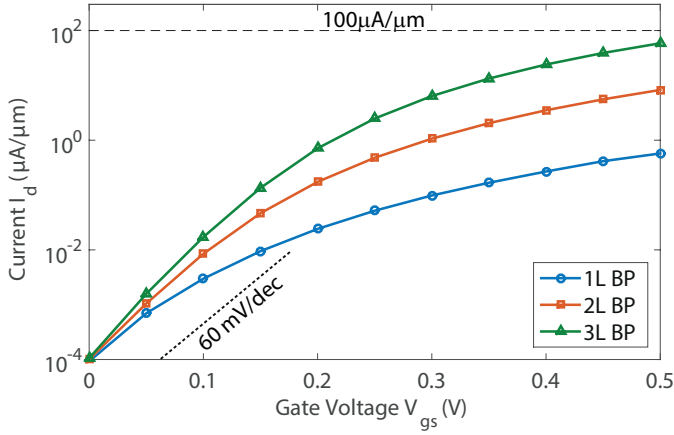


Fig. 8. Transfer characteristics $I_d - V_{gs}$ at $V_{ds} = 0.5$ V of single- (solid line with circles) double- (solid line with square), and triple-layer (solid line with triangles) BP TFETs.

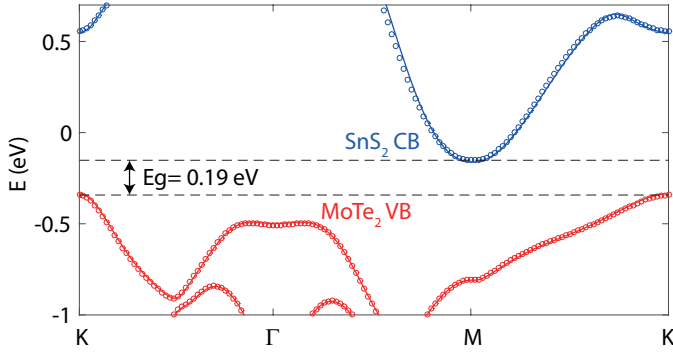


Fig. 9. Band structure of the MoTe₂-SnS₂ van der Waals heterojunction. The highest valence bands are formed by the MoTe₂ layer, the lowest conduction bands belong to the SnS₂ layer. Circles mark the results calculated with VASP, lines are from the MLWF Hamiltonian.

MoTe₂ monolayer with a $N_A=10^{13}$ cm⁻² acceptor concentration, the drain by a *n*-doped SL SnS₂ with a $N_D = 10^{13}$ cm⁻² donor concentration. The two layers overlap in the middle of the device over a 20 nm long region. The top and bottom gate contacts extend on both sides by 20 nm. The motivation behind the elongated gates is the desire to avoid tunneling paths at the edges of the overlap area and to orientate the transfer of electrons from one layer to the other along the vertical *z* direction. One layer of hexagonal Boron Nitride (BN) is deposited on top of the free-standing part of MoTe₂ to eliminate strong potential variations close to the interface edges. In effect, BN has a dielectric permittivity closer to both MoTe₂ and SnS₂ than HfO₂, the surrounding oxide. We use the same supply voltage $V_{DD} = 0.5$ V as before and set the OFF-current to $I_{OFF}=0.1$ nA/μm by adjusting the gate workfunctions. This makes the established results comparable to TMDs, novel 2-D materials, and few-layer BP.

MoTe₂ and SnS₂ are two semiconductors with relatively large band gaps for tunneling applications, 0.91 and 1.6 eV, respectively, but their stacking forms a staggered band alignment with a tunneling gap of only 0.19 eV. The band diagram of the MoTe₂-SnS₂ van der Waals heterojunction under flat band conditions is shown in Fig. 10 (b). The TFET operates by grounding the bottom gate and sweeping the top

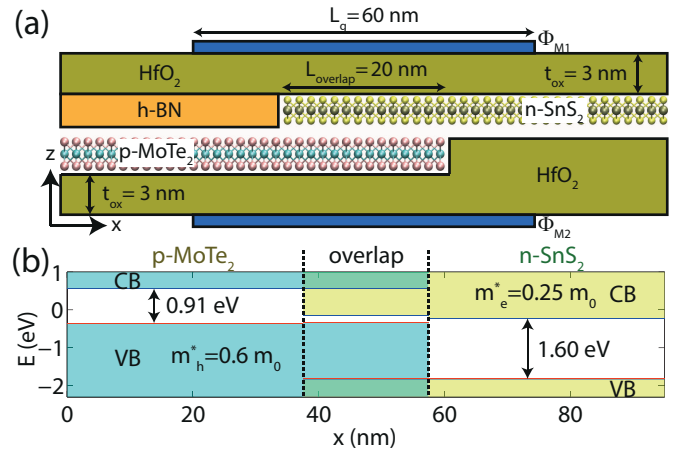


Fig. 10. (a) Schematic view of the considered double-gate MoTe₂-SnS₂ hetero-TFET. (b) Conduction and valence band profiles of the device along the transport axis under flat band conditions.

one. A vertical electric field is created by this process. In the ON-state, it pushes down the conduction band edge of SnS₂ below the valence band maximum of MoTe₂ because the potential close to the top layer is better controlled by the gate contact. This mechanism can be visualized in Fig. 11. At $V_{gs} = 0$ V the valence band maximum (VBmax) of MoTe₂ is at a lower energy than the conduction band minimum (CBmin) of SnS₂ in the active regions: there is no tunneling path. As the gate voltage increases, the CBmin of SnS₂ moves downwards faster than the VBmax of MoTe₂, closing the 0.19 eV gap between both materials. At $V_{gs}=0.25$ V, a narrow tunneling window appears in the middle of the device, but most of the current flows at the right edge of the overlap region, from MoTe₂ into the free-standing SnS₂ layer (point tunneling). In the ON-state, a large tunneling window is formed in the overlap area (line tunneling). It leads to a high ON-current $I_{ON}=130$ μA/μm, the tunneling length being the distance between both semiconducting layers, i.e. less than 0.5 nm. The sharp peaks observed in the ballistic transmission functions plotted in Fig. 11 result from the presence of resonance and anti-resonance states. The latter either enhance or deteriorate the transmission probability. The inclusion of a dissipative scattering mechanism such as electron-phonon interactions would either eliminate them or broaden their spectral width.

The role of the overlap length has also been investigated by simulating a TFET where this parameter is increased to 40 nm, twice as large as before. The original and modified devices deliver almost identical currents, as shown in Fig. 12. This suggests that the tunneling current is not homogeneously distributed over the overlap region. Indeed, a large contribution comes from the current at the right edge of the interface. Still, the constructed heterojunction achieves an ON-current $I_{ON}=130$ μA/μm, which is higher than the TFET relying on triple-layer BP and comparable to what is found for the studied novel 2-D semiconductors, as summarized in Table I. These results are very encouraging since the playground for van der Waals heterojunctions is almost infinite (material type and number of layers), especially if it is recalled that 1,800 2-D crystals might exist [19].

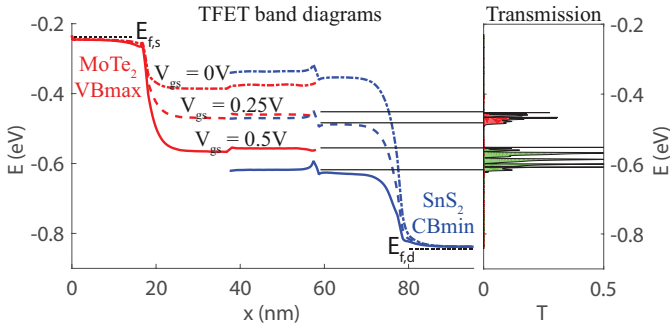


Fig. 11. Band diagram and energy-resolved transmission probability in the MoTe₂-SnS₂ TFET at various gate voltages. The valence band maximum (VBmax) of MoTe₂ and the conduction band minimum (CBmin) of SnS₂ are represented. The horizontal black lines mark the edges of the tunneling windows at 0.25 and 0.5 V gate voltages, encompassing the red and green transmission profiles, respectively.

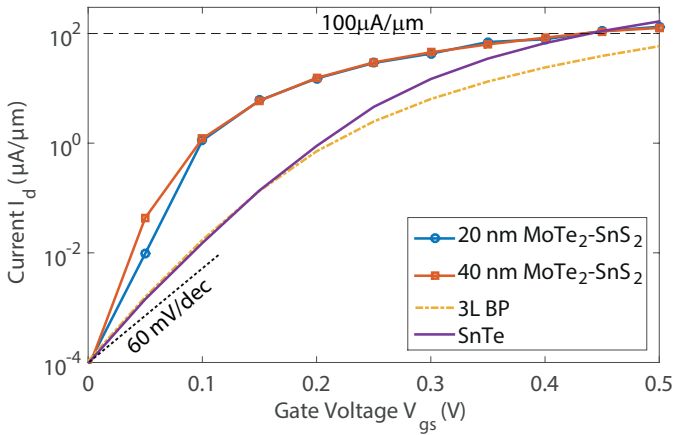


Fig. 12. Transfer characteristics $I_d - V_{gs}$ at $V_{ds}=0.5$ V of the MoTe₂-SnS₂ heterojunction TFETs with 20 (solid line with circles) and 40 nm (solid line with squares) overlap lengths. Triple-layer black phosphorus (dashed line) and SnTe (solid line) are shown for comparison.

IV. CONCLUSION

By performing atomistic quantum transport simulations based on first principles, we have demonstrated that single-layer transition metal dichalcogenides are not competitive as TFET channel materials. None of them, except for WTe₂, has a ON-current that exceeds $1 \mu\text{A}/\mu\text{m}$ at a supply voltage $V_{DD}=0.5$ V and $I_{OFF}=0.1$ nA/μm. However, several novel 2-D single-layer semiconductors that have just recently started to attract some attention could play a prominent role in future TFETs. Some of them such as SnTe, As, TiNBr, and Bi are predicted to deliver $I_{ON} > 100 \mu\text{A}/\mu\text{m}$. Extending the range of search to devices made of few-layer crystals may further improve the situation if the considered semiconductors have a low and direct band gap, small electron and hole effective masses, and their thickness remains narrow enough to maintain an excellent electrostatic control via the gate contact. A bright future can be envisioned for TFETs with a 2-D channel material as the design space is huge and components with significantly better performance than conventional TMDs have already been identified.

Nevertheless, there is a practical lower limit on the band gap in homojunction TFETs. It is imposed by the supply voltage.

	E_g (eV)	m_e^* (m_0)	m_h^* (m_0)	I_{ON} ($\mu\text{A}/\mu\text{m}$)
MoS ₂	1.67	0.46	0.56	5.9×10^{-3}
MoSe ₂	1.43	0.53	0.63	2.4×10^{-2}
MoTe ₂	1.06	0.54	0.68	5.5×10^{-1}
WS ₂	1.80	0.30	0.38	1.4×10^{-2}
WSe ₂	1.53	0.33	0.43	9.1×10^{-2}
WTe ₂	0.92	0.28	0.39	13.95
*HfSe ₂	0.76	0.19	0.14	2.3×10^{-2}
AlLiTe ₂	0.91	0.15	0.36	1.99
As	0.81	0.08	0.08	127.9
Bi	0.55	0.04	0.03	108.0
CrSe ₂	0.75	1.00	0.99	8.6×10^{-1}
SnTe	0.73	0.09	0.10	166.3
TiNBr	0.63	0.18	0.17	116.7
TiNCl	0.58	0.18	0.17	83.2
1L-BP	1.61	0.17	0.16	5.7×10^{-1}
2L-BP	1.09	0.18	0.16	8.3
3L-BP	0.79	0.16	0.14	58.6
MoTe ₂ -SnS ₂	0.19	0.25	0.6	130

* Indirect band gap

TABLE I
SUMMARY OF THE BAND GAPS (E_g), ELECTRON (m_e^*) AND HOLE EFFECTIVE MASSES (m_h^*) OF THE 2-D SEMICONDUCTORS CONSIDERED IN THIS WORK, AND COMPUTED TFET ON-CURRENTS (I_{ON}).

The materials presented here, in particular Bi, are already very close to this limit. Finding a 2-D semiconductor with a similar direct band gap, but lower electron and hole effective masses might lead to improved performance, but might not be sufficient to surpass what van der Waals heterojunctions can provide. A hetero-TFET with vertical transport can still be turned off with arbitrarily small staggered gap values, as long as the band gaps of the individual layers are reasonably large. The simulated MoTe₂-SnS₂ device is made of well-known 2-D compounds. In spite of that, it performs almost as well as the best homojunction TFETs using novel 2-D semiconductors as their channel. A better engineered hetero-TFET combining layers with smaller effective masses and a lower tunneling gap is likely to outperform all the examples explored in this paper. The next step is therefore to determine the most suitable material combinations for heterojunction TFETs from the large database of 2-D semiconductors.

V. ACKNOWLEDGMENTS

This work was supported by the MARVEL NCCR of the Swiss National Science Foundation and by ETH Grant ETH-32 15-1. We acknowledge PRACE for awarding us access to Piz Daint at CSCS under Project pr28.

REFERENCES

- [1] D. E. Nikonov and I. A. Young, "Benchmarking of beyond-cmos exploratory devices for logic integrated circuits," *IEEE Journal on Exploratory Solid-State Computational Devices and Circuits*, vol. 1, pp. 3–11, 2015.
- [2] A. M. Ionescu and H. Riel, "Tunnel field-effect transistors as energy-efficient electronic switches," *Nature*, vol. 479, p. 329, 2011.
- [3] R. Gandhi, Z. Chen, N. Singh, K. Banerjee, and S. Lee, "Cmos-compatible vertical-silicon-nanowire gate-all-around p-type tunneling fetts with ≤ 50 -mv/decade subthreshold swing," *IEEE Electron Device Letters*, vol. 32, no. 11, pp. 1504–1506, Nov 2011.
- [4] K. Tomioka, M. Yoshimura, and T. Fukui, "Steep-slope tunnel field-effect transistors using III-V nanowire/Si heterojunction," in *2012 Symposium on VLSI Technology (VLSIT)*, June 2012, pp. 47–48.

- [5] K. E. Moselund, H. Schmid, C. Bessire, M. T. Bjork, H. Ghoneim, and H. Riel, "InAs-Si nanowire heterojunction tunnel FETs," *Electron Device Letters, IEEE*, vol. 33, p. 1453, 2012.
- [6] G. Dewey, B. Chu-Kung, J. Boardman, J. M. Fastenau, J. Kavalieros, R. Kotlyar, W. K. Liu, D. Lubyshev, M. Metz, N. Mukherjee, P. Oakey, R. Pillarisetty, M. Radosavljevic, H. W. Then, and R. Chau, "Fabrication, characterization, and physics of III-V heterojunction tunneling field effect transistors (h-tfet) for steep sub-threshold swing," in *2011 International Electron Devices Meeting*, Dec 2011, pp. 33.6.1–33.6.4.
- [7] B. Rajamohanam, R. Pandey, V. Chobpattana, C. Vaz, D. Gundlach, K. P. Cheung, J. Suehle, S. Stemmer, and S. Datta, "0.5 V Supply Voltage Operation of In_{0.65}Ga_{0.35}As/GaAs_{0.4}Sb_{0.6} Tunnel FET," *IEEE Electron Device Letters*, vol. 36, no. 1, pp. 20–22, Jan 2015.
- [8] D. Mohata, B. Rajamohanam, T. Mayer, M. Hudait, J. Fastenau, D. Lubyshev, A. W. K. Liu, and S. Datta, "Barrier-engineered arsenide-antimonide heterojunction tunnel FETs with enhanced drive current," *Electron Device Letters, IEEE*, vol. 33, p. 1568, 2012.
- [9] E. Memisevic, M. Hellenbrand, E. Lind, A. R. Persson, S. Sant, A. Schenk, J. Svensson, R. Wallenberg, and L.-E. Wernersson, "Individual defects in InAs/InGaAsSb/GaSb nanowire tunnel field-effect transistors operating below 60 mV/decade," *Nano Letters*, vol. 17, pp. 4373–4380, 2017.
- [10] B. Radisavljevic, A. Radenovic, J. Brivio, V. Giacometti, and A. Kis, "Single-layer MoS₂ transistors," *Nat Nano*, vol. 6, p. 147, 2011.
- [11] A. K. Geim and I. V. Grigorieva, "Van der Waals heterostructures," *Nature*, vol. 499, p. 419, 2013.
- [12] H. Ilatikhameneh, Y. Tan, B. Novakovic, G. Klimeck, R. Rahman, and J. Appenzeller, "Tunnel field-effect transistors in 2-d transition metal dichalcogenide materials," *IEEE Journal on Exploratory Solid-State Computational Devices and Circuits*, vol. 1, pp. 12–18, 2015.
- [13] R. Ghosh and S. Mahapatra, "Monolayer transition metal dichalcogenide channel-based tunnel transistor," *Electron Devices Society, IEEE Journal of the*, vol. 1, p. 175, 2013.
- [14] T. A. Ameen, H. Ilatikhameneh, G. Klimeck, and R. Rahman, "Few-layer phosphorene: An ideal 2d material for tunnel transistors," *Scientific Reports*, vol. 6, p. 28515, 2016.
- [15] K.-T. Lam, X. Cao, and J. Guo, "Device performance of heterojunction tunneling field-effect transistors based on transition metal dichalcogenide monolayer," *Electron Device Letters, IEEE*, vol. 34, p. 1331, 2013.
- [16] A. Szabo, S. Koester, and M. Luisier, "Metal-dichalcogenide heterotransistors: Are they a viable option for low power electronics?" in *Device Research Conference (DRC), 2014 72nd Annual*, 2014, p. 19.
- [17] D. Sarkar, X. Xie, W. Liu, W. Cao, J. Kang, Y. Gong, S. Kraemer, P. M. Ajayan, and K. Banerjee, "A subthermionic tunnel field-effect transistor with an atomically thin channel," *Nature*, vol. 526, p. 91, 2015.
- [18] Y. Balaji, Q. Smets, C. J. L. de la Rosa, A. K. A. Lu, D. Chiappe, T. Agarwal, D. Lin, C. Huyghebaert, I. Radu, D. Mocuta, and G. Groeseneken, "Tunneling transistors based on mos₂/mote₂ van der waals heterostructures," *IEEE Journal of the Electron Devices Society*, vol. PP, no. 99, pp. 1–1, 2018.
- [19] N. Mounet, M. Gibertini, P. Schwaller, D. Campi, A. Merkys, A. Marrazzo, T. Sohier, I. E. Castelli, A. Cepellotti, G. Pizzi, and N. Marzari, "Novel two-dimensional materials from high-throughput computational exfoliation of experimentally known compounds," *Nature Nanotechnology*, vol. 13, p. 246, 2018.
- [20] W. Kohn and L. J. Sham, "Self-consistent equations including exchange and correlation effects," *Phys. Rev.*, vol. 140, pp. A1133–A1138, 1965.
- [21] G. Kresse and J. Furthmüller, "Efficient iterative schemes for ab initio total-energy calculations using a plane-wave basis set," *Phys. Rev. B*, vol. 54, p. 11169, 1996.
- [22] J. P. Perdew, K. Burke, and M. Ernzerhof, "Generalized gradient approximation made simple," *Phys. Rev. Lett.*, vol. 77, pp. 3865–3868, 1996.
- [23] L. Liu, S. Bala Kumar, Y. Ouyang, and J. Guo, "Performance limits of monolayer transition metal dichalcogenide transistors," *Electron Devices, IEEE Transactions on*, vol. 58, p. 3042, 2011.
- [24] J. Heyd, G. E. Scuseria, and M. Ernzerhof, "Erratum: "hybrid functionals based on a screened coulomb potential" [j. chem. phys.118, 8207 (2003)]," *The Journal of Chemical Physics*, vol. 124, no. 21, 2006.
- [25] D. Y. Qiu, F. H. da Jornada, and S. G. Louie, "Optical spectrum of mos₂: Many-body effects and diversity of exciton states," *Phys. Rev. Lett.*, vol. 111, p. 216805, 2013.
- [26] S. Grimme, J. Antony, S. Ehrlich, and H. Krieg, "A consistent and accurate ab initio parametrization of density functional dispersion correction (DFT-D) for the 94 elements H-Pu," *The Journal of Chemical Physics*, vol. 132, 2010.
- [27] N. Marzari and D. Vanderbilt, "Maximally localized generalized Wannier functions for composite energy bands," *Phys. Rev. B*, vol. 56, p. 12847, 1997.
- [28] M. Luisier, A. Schenk, W. Fichtner, and G. Klimeck, "Atomistic simulation of nanowires in the $sp^3d^5s^*$ tight-binding formalism: From boundary conditions to strain calculations," *Phys. Rev. B*, vol. 74, p. 205323, 2006.
- [29] A. Szabó, R. Rhyner, and M. Luisier, "Ab initio simulation of single- and few-layer MoS₂ transistors: Effect of electron-phonon scattering," *Phys. Rev. B*, vol. 92, p. 035435, 2015.
- [30] A. Szabo, "Dissipative quantum transport simulations in two-dimensional semiconductor devices from first principles," Ph.D. dissertation, ETH Zürich, 2016.
- [31] A. Szabo, S. J. Koester, and M. Luisier, "Ab-Initio Simulation of van der Waals MoTe₂-SnS₂ Heterotunneling FETs for Low-Power Electronics," *IEEE Electron Device Letters*, vol. 36, pp. 514–516, 2015.
- [32] A. K. A. Lu, M. Houssa, I. P. Radu, and G. Pourtois, "Toward an understanding of the electric field-induced electrostatic doping in van der waals heterostructures: A first-principles study," *ACS Appl. Mater. Interfaces*, vol. 9, pp. 7725–7734, 2017.
- [33] A. Kumar and P. Ahluwalia, "Tunable dielectric response of transition metals dichalcogenides mx₂ (m=mo, w; x=s, se, te): Effect of quantum confinement," *Physica B: Condensed Matter*, vol. 407, no. 24, pp. 4627–4634, 2012.
- [34] T. Sohier, M. Calandra, and F. Mauri, "Two-dimensional fröhlich interaction in transition-metal dichalcogenide monolayers: Theoretical modeling and first-principles calculations," *Phys. Rev. B*, vol. 94, p. 085415, 2016.
- [35] H. Ilatikhameneh, R. B. Salazar, G. Klimeck, R. Rahman, and J. Appenzeller, "From fowler-nordheim to non-equilibrium green's function modeling of tunneling," *IEEE Transactions on Electron Devices*, vol. 63, pp. 2871–2878, 2016.
- [36] J. Qiao, X. Kong, Z.-X. Hu, F. Yang, and W. Ji, "High-mobility transport anisotropy and linear dichroism in few-layer black phosphorus," *Nat. Commun.*, vol. 5, p. 4475, 2014.
- [37] A. Szabo, R. Rhyner, H. Carrilo-Nunez, and M. Luisier, "Phonon-limited performance of single-layer, single-gate black phosphorus n- and p-type field-effect transistors," in *Electron Devices Meeting (IEDM), 2015 IEEE International*, 2015, p. 12.1.